Electric Power Systems Research 202 (2022) 107595

Contents lists available at ScienceDirect

Electric Power Systems Research

journal homepage: www.elsevier.com/locate/epsr

DC grid controller for optimized operation of voltage source converter based multi-terminal HVDC networks

Grain Philip Adam [a,*], Fahad Alsokhiry [b], Ahmed Alabdulwahab [b]

[a] NEOM, Riyadh, P.O. Box 10, Riyadh 11411, Saudi Arabia
[b] Department of Electrical and Computer Engineering, King Abdulaziz University, Jeddah 21589, Saudi Arabia

ARTICLE INFO

Index Terms:
High-voltage direct current transmission grids
Modular multilevel converter
Power loss minimization
Security constrained optimization

ABSTRACT

Generally, multi-terminal dc grids provide full control over the dc powers that converter terminals exchange with their respective host ac grids. Nevertheless, the same level of controllability does not exist over the power flow in the individual dc lines of a highly meshed HVDC network, and this increases the risk of overloading the dc cables that present lower resistances. To address the highlighted shortcoming, this paper presents a generic dc grid controller that uses nonlinear constrained optimization to optimize the performance of multi-terminal HVDC networks for any desirable operational objective, within system physical constraints such as dc cable and converter thermal limits, and minimum and maximum dc voltage limits. The presented dc grid controller performs online optimization at regular intervals to dynamically estimate and update the set-points of the converter terminals as system operating conditions vary. The technical viability of the proposed controller is assessed using a generic seven-terminal HVDC network that uses voltage sourced modular multilevel converters. Simulations from the scenarios that prioritize dc grid power loss or operational cost minimization show that the presented dc grid controller exhibits good performance during normal operation as converter terminals set-points vary, and during dc grid reconfiguration following simulated successive outages of the dc cables. It has been shown that the performance of the proposed DC grid control is not affected by the parameter variation such as changes of resistance with temperature.

1. Introduction

Rapid development of large-scale and remote renewable power generations from consumption centres have strengthened the business case for multi-terminal high-voltage direct current (MT-HVDC) network [1–3]. This has led to significant investments in research from industry and academia to develop technologies that can address the outstanding challenges of MT-HVDC networks[4–6]. Such MT-HVDC networks provide efficient platforms for large power exchange over wide geographical areas, with improved control flexibilities and utilization of power corridors compared to equivalent HVAC networks[7, 8]. Modular multilevel converters (MMCs) are well-suited for MT-HVDC grids due to the following reasons [8–14]: ease of scalability to high-power and ultra-high-voltage; resilient to internal faults; independent control of active and reactive powers; and seamless power reversal is achievable without significant disruption to the power flow throughout the dc network or any other converter terminals. These attributes have attracted extensive researches in different aspects of voltage sourced converter (VSC) based MT-HVDC networks such as coordinated control and protection strategies for continued operation during ac and dc network faults [12, 15, 16], and the quest for a new class of converter topologies with increased control range and flexibility [6, 17, 18].

Amongst several control methods of MT-HVDC networks discussed in the literature, the conventional method in which one converter terminal sets the dc voltage level for the entire grid while the remaining converter terminals regulate the amounts of active powers being exchanged with their respective ac grids is the most straightforward and widely reported [19–22]. In this control method, the dc voltage controlling converter operates as slack bus and must be capable of supplying the power mismatch between the supply and demand of all other converter terminals. Failure of the dc voltage controlling converter can cause system collapse if adequate countermeasures are not put in place.

Master-slave control method described in [23] minimizes the risk of the conventional control method by quickly re-allocating the dc voltage control function to a new converter. It modifies the implementation of the active power regulator such that it acts as a dc voltage regulator

* Corresponding author. Grain Philip Adam, 1/2 8 Slatefield Street, Glasgow, G31 1UA, UK.
E-mail address: grain.adam@neom.com (G.P. Adam).

https://doi.org/10.1016/j.epsr.2021.107595
Received 27 March 2021; Received in revised form 13 August 2021; Accepted 14 September 2021
Available online 6 October 2021

when its dc voltage hits the upper or lower limits. In this way, the severe transient over-voltage/under-voltage problem of conventional voltage margin method during re-allocation of the dc voltage control function to new converter could be avoided [24–29].

Droop control method is widely used with MT-HVDC networks [30–32], and it has been applied in two multi-terminal dc grids in China, Nanao project and Zhoushan projects. Its main attributes are: it permits participation of multiple converters to dc grid voltage regulation, and appreciated for its stability and resiliency to converter outage and abrupt changes in active power set-points. However, it is only applicable to converters operate in strong ac grids that can sink or source the rated active power, without causing significant stability problems [10].

Although the above methods offer some level of controllability over dc or active power injection at converter terminals, they do not possess the ability to force the dc powers toward the desirable paths in the dc grid; therefore, unable to prevent overloading of the dc cables and dc voltage controlling converters or ensure optimal utilization of dc grid infrastructures.

Several series current/power flow controllers or devices have been proposed in recent years, with the aim of preventing dc lines overload through by manipulation of the dc line voltage drops to instigate forced distribution of the dc power flows between multiple dc paths/lines according to predefined set-points or criteria[5, 33–36]. In this way, the power flows in dc lines that contain series current/power flow controlling devices can be controlled arbitrarily (magnitude and direction). The effectiveness of these devices have been tested and validated under normal and abnormal conditions[36–39]; nonetheless, they add cost and require space.

Therefore, this paper presents a generic dc grid controller that performs online constrained optimization to dynamically estimate and update the optimal set-points of converter terminals of the dc grid for a predefined operational objective. Sensitivity analysis is carried out to examine the robustness of the proposed dc grid controller against the drift in the resistances of the dc cables as temperature changes. An additional objective function that minimizes the generation cost is also presented for completeness only. The main features of the presented dc grid controller are:

- Can be extended to MT-HVDC grids with large number of converter terminals, independent of grid and converter topologies.
- It does not significantly affect online calculations during real-time or co-simulation as the optimized set-points in previous sampling period are re-used as initial conditions in the present sampling period. Therefore, it can be incorporated within EMT (electromagnetic transient) and RMS (root mean square or simply phasor) environments, independent of the extent of the details of converters representation or modeling.
- Permits incorporation of all equality and inequality constraints such as thermal limits of the dc cables and converters. Also, ac side constraints could be included; however, is not covered in this paper for simplicity.

The rest of the paper is organized as follows: Section 2 describes the fundamentals that underpin the proposed dc grid controller or optimizer, and mathematical formulations with the aid of two illustrative objective functions and associated equality and inequality constraints that define the system technical boundaries. Also, it describes the per phase averaged voltage source converter or MMC model employed in this paper to simulate each converter station and associated control systems. Section 2 evaluates performance of the proposed dc grid controller/optimizer under two different objective functions that minimize transmission losses and generation cost, and assesses its vulnerability to system parameter variations. Section 4 summarizes and contextualizes the overall finings of this paper.

2. The proposed optimized operation

2.1. DC grid optimizer

This section presents the dc grid controller capable of optimizing the operation of complex VSC based multi-terminal HVDC network for different desirable operational objectives, during normal operation and after dc grid reconfiguration following dc cable or converter outage. The presented dc grid controller performs constrained optimization over regular time span 'T_m' in order to estimate the optimal set-points of the converter terminals. To speed up optimization process, the optimized set-points at time '$t= kT_m$' are used as initial conditions at next sample time '$t=(k+1)T_m$'. This means if the set-points remain unchanged, each optimization process requires only one iteration. For ease of illustration, a meshed multi-terminal HVDC network employing VSCs shown in Fig. 1 is analyzed in this paper, with all converter terminals assumed to be lossless. The directions of the active powers, and dc powers and dc currents displayed in Fig. 1 are assumed to be positive. As the electromagnetic transients in the dc side is not relevant in such studies thus can be ignored, the instantaneous dc currents and dc powers that converter terminals inject into dc node B_i (where, $i = 1$ to N_{dc}, and N_{dc} represents the number of dc link nodes) are:

$$I_{dci}(t) = \sum_{j=1}^{N_{dc}} G_{ij} V_{dcj}(t) \tag{1}$$

$$P_{dci}(t) = V_{dci}(t) I_{dci}(t) = \sum_{j=1}^{N_{dc}} G_{ij} V_{dci}(t) V_{dcj}(t). \tag{2}$$

The term G_{ij} in (1) represents the element of conductance matrix which is formulated, considering the status of dc circuit breakers 'μ_{ij}' at the ends of the dc cables between the dc nodes 'i' and 'j'. $\mu_{ij} = 1$ when the dc line between the dc nodes 'i' and 'j' is in service with both sets of dc circuit breakers at its ends are closed, and $\mu_{ij} = 0$ when the dc line between the dc nodes 'i' and 'j' is out of service and both sets of dc circuit breakers at its ends are opened. For computational reasons, incorporation dc circuit breaker status in conductance matrix is realized by setting $\sigma_{ij} = 10^6$ and $10e^{-6}$ when μ_{ij} are 0 and 1 respectively. For examples, $G_{11} = \sigma_{12}/R_{12} + \sigma_{13}/R_{13} + \sigma_{14}/R_{14}$ and $G_{12} = -\sigma_{12}/R_{12}$; where R_{ij} represents the resistance of the dc cable between the dc nodes 'i' and 'j'. The instantaneous dc current flow in each dc line that connects two dc nodes 'i' and 'j' is:

$$I_{dcij}(t) = G_{ij}\left[V_{dci}(t) - V_{dcj}(t)\right] \tag{3}$$

The total instantaneous power loss in the dc network is expressed as:

$$P_L(t) = \frac{1}{2}\sum_{i=1}^{N_{dc}}\sum_{j=1}^{N_{dc}} \left|G_{ij}\right|\left[V_{dci}(t) - V_{dcj}(t)\right]^2. \tag{4}$$

Some of the converter terminals of any multi-terminal HVDC networks are expected to have pre-defined power demand being imposed by dispatch or control center. This paper optimizes the HVDC network operation with minimum dc power losses considering strict constraints such as maximum and minimum current capability of each dc cable and dc voltage at each dc node as:

$$-I_{dcij\max} \le I_{dcij}(t) \le I_{dcij\max} \tag{5}$$

$$V_{dc\min} \le V_{dci}(t) \le V_{dc\max} \tag{6}$$

where, $I_{dcijmax}$ represents the maximum current rating of the dc cable between the dc nodes 'i' and 'j' for continuous operation, and V_{dcmax} and V_{dcmin} are the maximum and minimum allowable dc voltage limits for each dc node respectively. Additionally, the maximum and minimum dc power capability of the converters with unspecified power demand are considered as inequality constraints:

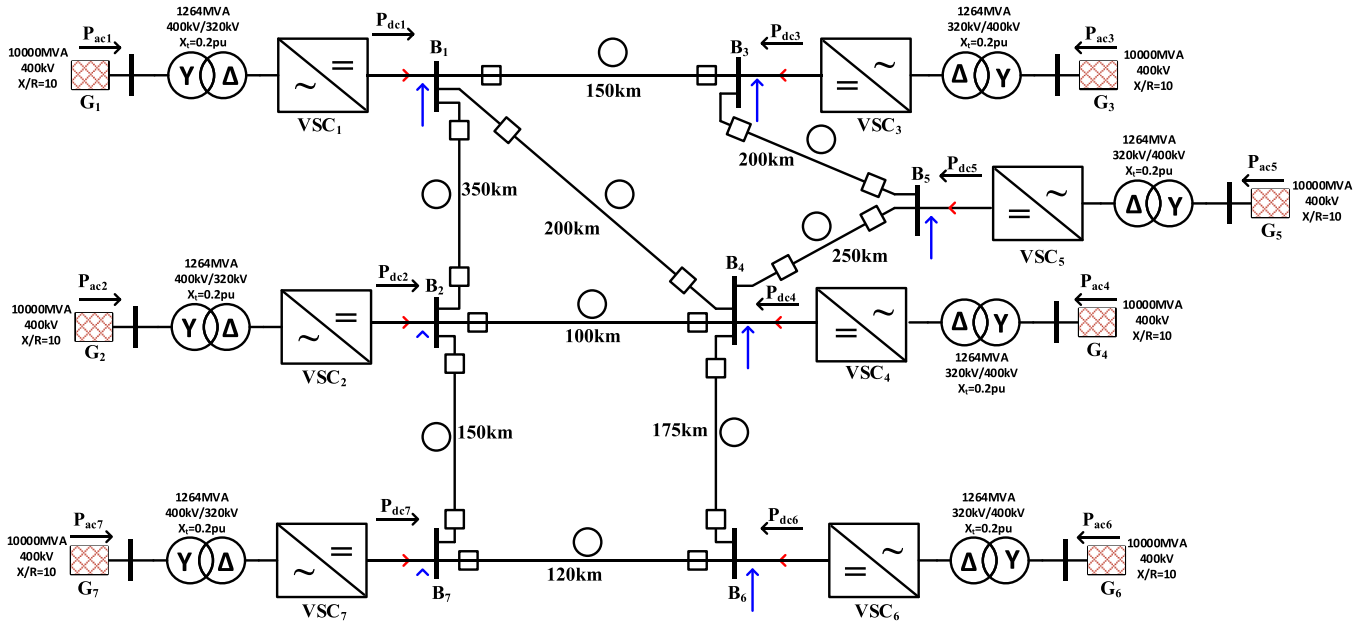

Fig. 1. Illustrative meshed VSC multi-terminal HVDC network.

$$P_{dc\min} \le P_{dci}(t) \le P_{dc\max} \tag{7}$$

where, P_{dcmax} and P_{dcmin} are the maximum and minimum dc power for continuous operation of the converter terminal.

In the additional example that examines minimization of the running cost of generic multi-terminal HVDC network in Fig. 1, the cost of generation mixed at ac networks 1, 2 and 5 (without specified power demands and available for optimization) are assumed to be quadratic functions of the form:

$$C_i = a_i + b_i|P_{dci}| + c_i P_{dci}^2 \tag{8}$$

Total net cost of running the multi-terminal HVDC network in Fig. 1 can be approximated, taking into account the polarity of dc powers (export or import) as:

$$C_T = \sum_{k=1}^{N_{dc}} \text{sign}(P_{dck}) \times C_k \tag{9}$$

Since the objective function in (9) is not a positive definite, it has been modified as in (10) to facilitate solution as a convex problem:

$$C_T^m = C_T^2 = \left[\sum_{k=1}^{N_{dc}} \text{sign}(P_{dck}) \times C_k\right]^2 \tag{10}$$

To implement the optimized dc grid controller for the system in Fig. 1, it is assumed that the power demands of converter terminals 3, 4, 6 and 7 are known, and the dc voltage of the converter terminal 1 is known and fixed at the rated value of 640 kV. Thus, the optimization formulation aims to find the set of parameters describe by column vector $\mathbf{y}(t) = [V_{dc2}(t), V_{dc3}(t), V_{dc4}(t), V_{dc5}(t), V_{dc6}(t), V_{dc7}(t), P_{dc1}(t), P_{dc2}(t), P_{dc5}(t)]^T$ that minimizes the objective function in (4) or (10), subject to equality constraints described by (2), and inequalities in (5), (6) and (7). The aforementioned optimization problem is expressed mathematically in a compact form as:

$$\min P_L(\mathbf{y}(t), \mathbf{u}(t)) \tag{11}$$

Subject to:

$$g_i(\mathbf{y}(t), \mathbf{u}(t)) = 0, i = 1, \ldots . m_e \tag{12}$$

$$h_k(\mathbf{y}(t), \mathbf{u}(t)) \le 0 k = 1, \ldots . m_c \tag{13}$$

where, g_i and h_k are equality and inequality constraints; m_e and m_c stand for the number of equality and inequality constraints; and $\mathbf{u}(t)$ is a column vector of input variables or simply pre-defined set-points, i.e., $\mathbf{u}(t) = [V_{dc1}(t), P_{dc3}(t), P_{dc4}(t), P_{dc6}(t), P_{dc7}(t)]^T$.

Therefore, an online solution of optimization problem described by (11), (12) and (13) provides updates for the set-points of the converter terminal. In this paper, optimization is performed and converter set-points are updated at the rate of 1 kHz (every 1 ms).

2.2. System modeling and control

Each converter terminal in Fig. 1 is modelled using an enhanced MMC average model in Fig. 3 [40, 41], where the subscript 'x' stands for phase legs 'a', 'b' or 'c', and '1' and '2 attached to 'x' refer to the upper and lower arms. For example, when 'x' is replaced by 'a', $i_{arm\_a1}(t)$ and $i_{arm\_a2}(t)$ represent the upper and lower arm currents of phase leg 'a', and similarly, phase 'a' upper and lower arm voltages $v_{arm\_a1}(t)$ and $v_{arm\_a2}(t)$, equivalent capacitor currents $i_{cap\_a1}(t)$ and $i_{cap\_a2}(t)$, and capacitor voltages $v_{cap\_a1}(t)$ and $v_{cap\_a2}(t)$. In the enhanced MMC average model in Fig. 3, phase 'a' upper and lower arm voltages and equivalent capacitor voltages are calculated as:

$$\begin{aligned} v_{arm\_a1}(t) &= \gamma_{a1} \times v_{cap\_a1} \\ v_{arm\_a2}(t) &= \gamma_{a2} \times v_{cap\_a2} \end{aligned} \tag{14}$$

$$\begin{aligned} i_{cap\_a1}(t) &= \gamma_{a1} \times i_{arm\_a1} \\ i_{cap\_a2}(t) &= \gamma_{a2} \times i_{arm\_a2} \end{aligned} \tag{15}$$

In (14) and (15), $\gamma_{a1}(t) = \frac{1}{2}[1\text{-}msin(\omega t+\delta)]$ and $\gamma_{a2}(t) = \frac{1}{2}[1+msin(\omega t+\delta)]$ represent phase 'a' upper and lower arms modulating functions, m is modulation index, ω is supply angular frequency and δ is the phase shift.

Fig. 2 displays the control systems implemented in each converter station in Fig. 1, which consists of the following controllers: selectable active power/or enhanced dc voltage with dc power droop on the most outer loop of the D-axis; reactive power on the most outer loop of the q-axis; fundamental output currents in synchronous D-q frame; and circulating current suppression in abc frame with the aid of proportional resonance controllers. With all converter terminals assumed to be lossless, $P_{dcj}(t)=P_{acj}(t)$ for all $j = 1$to7 As the dc grid optimizer described earlier estimates the optimal dc powers and dc voltages of all converter

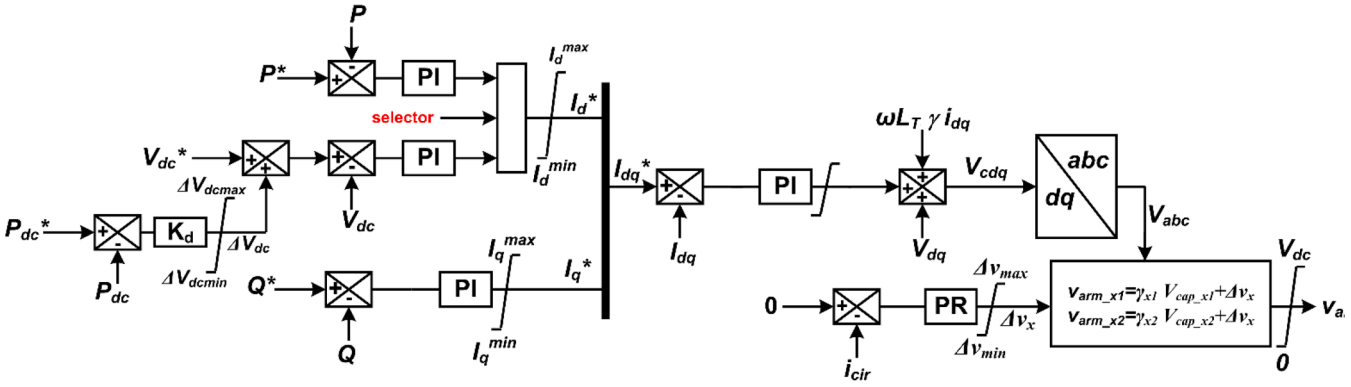

Fig. 2. Block diagram that depicts control system incorporated into each converter terminal of the test system in Fig. 1.

terminals, stable operation of multi-terminal HVDC network in Fig. 1 can be achieved when 'n_x' ($1 \leq n_x < N_{con}$) converter stations operate in dc voltage regulator (DCVR) mode and remaining 'N_{con}-n_x' converters operate in active power regulator (APR) mode. However, in this paper, all converters are operated in dc voltage control mode (i.e., $n_x = N_{con}$) with dc power droop as supplementary controller as shown in Fig. 2. The multi-terminal HVDC network system in Fig. 1 is modelled in MATLAB-SIMULINK, with power circuit and control implemented using Simulink and power systems library, while the dc grid optimizer is implemented using MATLAB m-files and S-function.

For simplicity, each dc circuit breaker in Fig. 1 is modelled with ideal switch in parallel with 10MΩ resistance. The parameters of the test system in Fig. 1 are displayed in

Table I. Throughout this paper, the minimum and maximum dc voltages, converter dc power and dc cable thermal limits are: $|V_{dci} - 640| \leq 32$kV, $|P_{dck}| \leq 1320$MW and $|I_{dcij}| \leq 2.5$kA respectively. Fig. 4 shows the high-level block diagram that depicts the data exchange and overall implementation of the presented dc grid controller. Data of the ac networks 1, 2 and 3 used for minimization of the running cost of the multi-terminal HVDC network in Fig. 1 are displayed in Table II.

Fig. 3 summarizes the overall implementation of the proposed dc grid controller and shows high-level depiction of different interfaces between the optimization stage, control system and dc grid power circuit. The new variables shown in Fig. 3 are defined in the caption of Fig. 3.

3. Performance evaluation

This section assesses the proposed optimization based dc grid controller described in Section 2.1, considering normal operation and dc network reconfiguration following multiple dc cables outage.

Table I
Simulation parameters of the test system in Fig. 1.

Converter parameters	
Rated dc voltage	640kV
Rated dc or active power	1200MW
Rated reactive power	±400MW
Rated line-to-line ac voltage	320kV
Arm inductance (L_{sm})	50mH
Equivalent cell capacitance (C_{sm})	46μF
Converter transformer	
Rated apparent power	1265MVA
Primary voltage	400kV
Secondary voltage	320kV
Leakage reactance	20%
DC line parameters	
Line resistance (R_{dc})	0.01Ω/km
Line inductance (L_{dc})	1.1mH/km
Line capacitance (C_{dc})	0.15μF/km

Table II.
Summary of the cost of power exports and imports at ac grids 1 to 7 (for illustration only).

	a_i (€/h)	b_i (€/MWh)	c_i(€/MW^{2}h)
$C_{1,3}$	750	20	0.055
$C_{2,4}$	3000	12	0.0425
$C_{5,6,7}$	1600	10	0.06

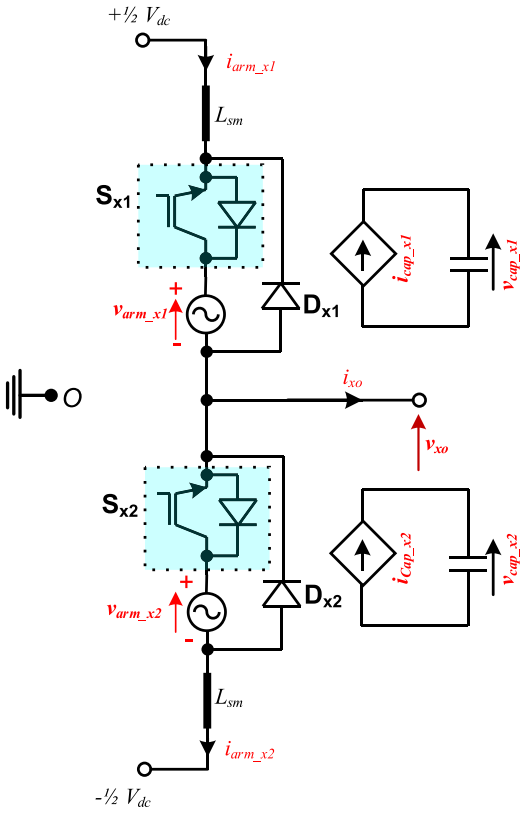

Fig. 3. Per phase averaged model of half-bridge modular multilevel converter employed in each converter terminal in Fig. 1.

3.1. Normal operation

In this assessment, all converter terminals are operated at unity power factor, and the dc power commands of the converter terminals with prescribed power demands (VSC_3, VSC_4, VSC_6 and VSC_7) are summarized as follows:

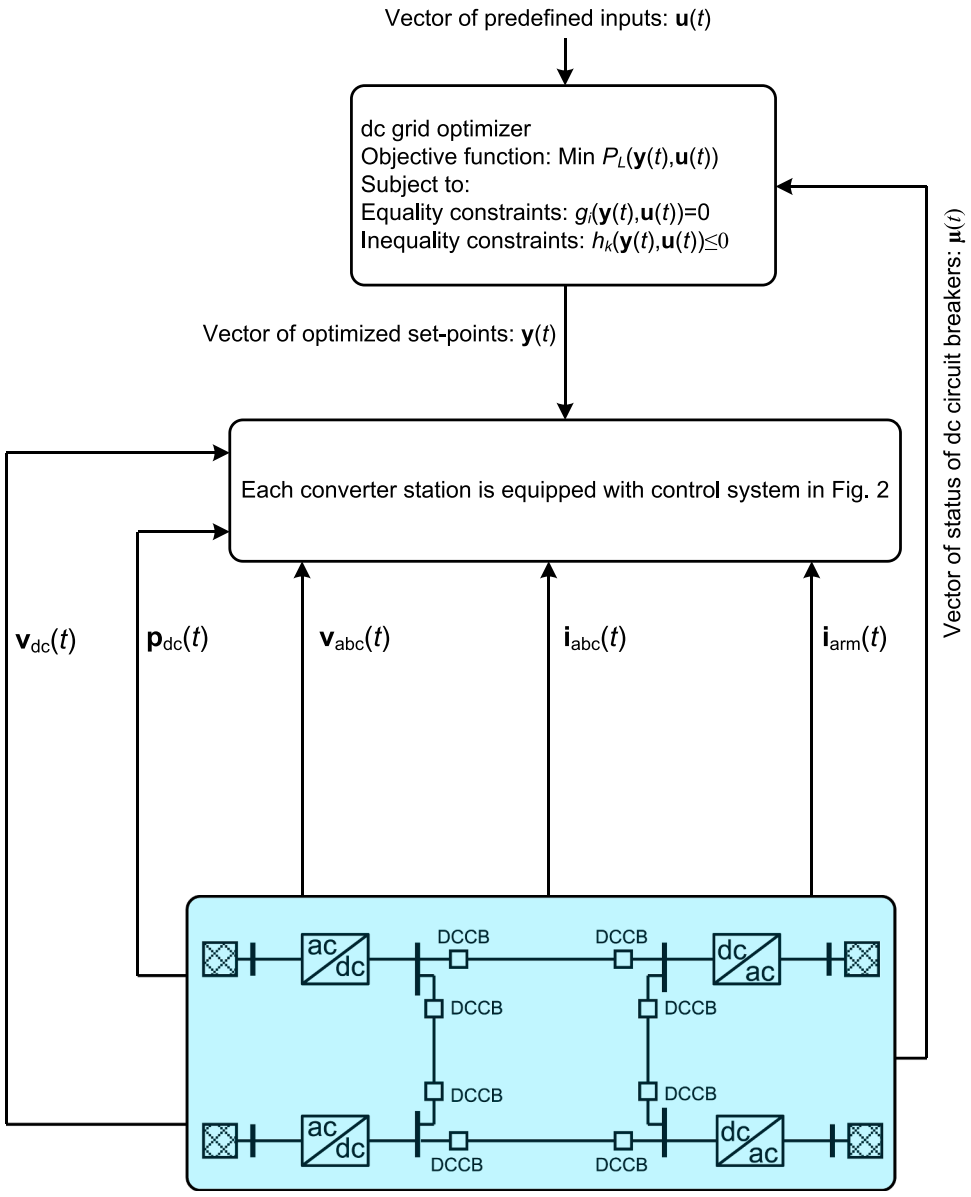

Fig. 4. Generic representation of the proposed optimization based dc grid controller, where $v_{dc}(t)$ and $p_{dc}(t)$ denote vectors of dc voltages and powers of the power converters, $v_{abc}(t)$ and $i_{abc}(t)$ denote vectors of three-phase ac voltages and currents at point-of-common couplings of the converter stations, and i_{arm} represents vector of arm currents of the converter stations.

- Initially, the dc powers of all converter terminals are held at zero, and at time $t = 0.5$ s, VSC3 ramps up its dc power gradually, from 0 to 1152MW, and its dc power is maintained at 1152MW for the rest of simulation period.
- At $t = 1$ s, VSC4 increases its dc power from 0 to 1200MW, and $t =$ 2.5 s, VSC4 decreases its dc power from 1200MW to −960MW, and then maintains its dc power at −960MW to the end of the simulation time.
- At $t = 1.5$ s, VSC6 ramps down its dc power from 0 to −300MW, and maintains its dc power at −300MW to the end of the simulation time.
- At time $t = 0.5$ s, VSC7 increases its dc power output gradually from 0 to 1200MW and maintains its dc power at 1200MW for the rest of simulation period.

The rates of power ramping up/down for all the cases are set at +/-1200MW/125 ms. Fig. 5 displays the simulation waveforms that illustrate the response of the presented optimization based dc controller as the power set-points of the converters VSC_3, VSC_4, VSC_6 and VSC_7 vary as stated above. Fig. 5(a) and (b), and (c) and (d) present the measured dc powers and dc voltages of the converter terminals VSC_1 through VSC_7 superimposed on the theoretical optimal dc powers and dc voltages estimated by the dc grid controller. The solid and dotted lines in Fig. 5(a) to (d) referred to the measured and estimated optimal dc powers and dc voltages respectively. These waveforms indicate that the multi-terminal HVDC network in Fig. 1 operate satisfactorily, and the presented dc grid controller is able to adjust the theoretical estimates of the optimal dc powers and voltages with sufficient speed and accuracy as power demands vary, see Fig. 5(a) to (d). Because the tracking accuracy and speed of the power set-points are greatly influenced by the droop or proportional term K_d (P_{dc}*-P_{dc}) in Fig. 2, limited overshoots are observed in the measured dc voltages as the power set-points vary, see Fig. 5(c) and (d). The current flow in the dc cables are shown in Fig. 5(e) and (f), and the positive direction of current flow is assumed to be from node '*i*' to '*j*' when the dc current in the dc cable is expressed as $I_{dcij}(t)$. Notice that as VSC_3 ramps up its power injection into dc grid from 0 to 1152MW during $0.5s \leq t \leq 1$ *s*, VSC_1 and VSC_5 act as dc power balancer and total dc

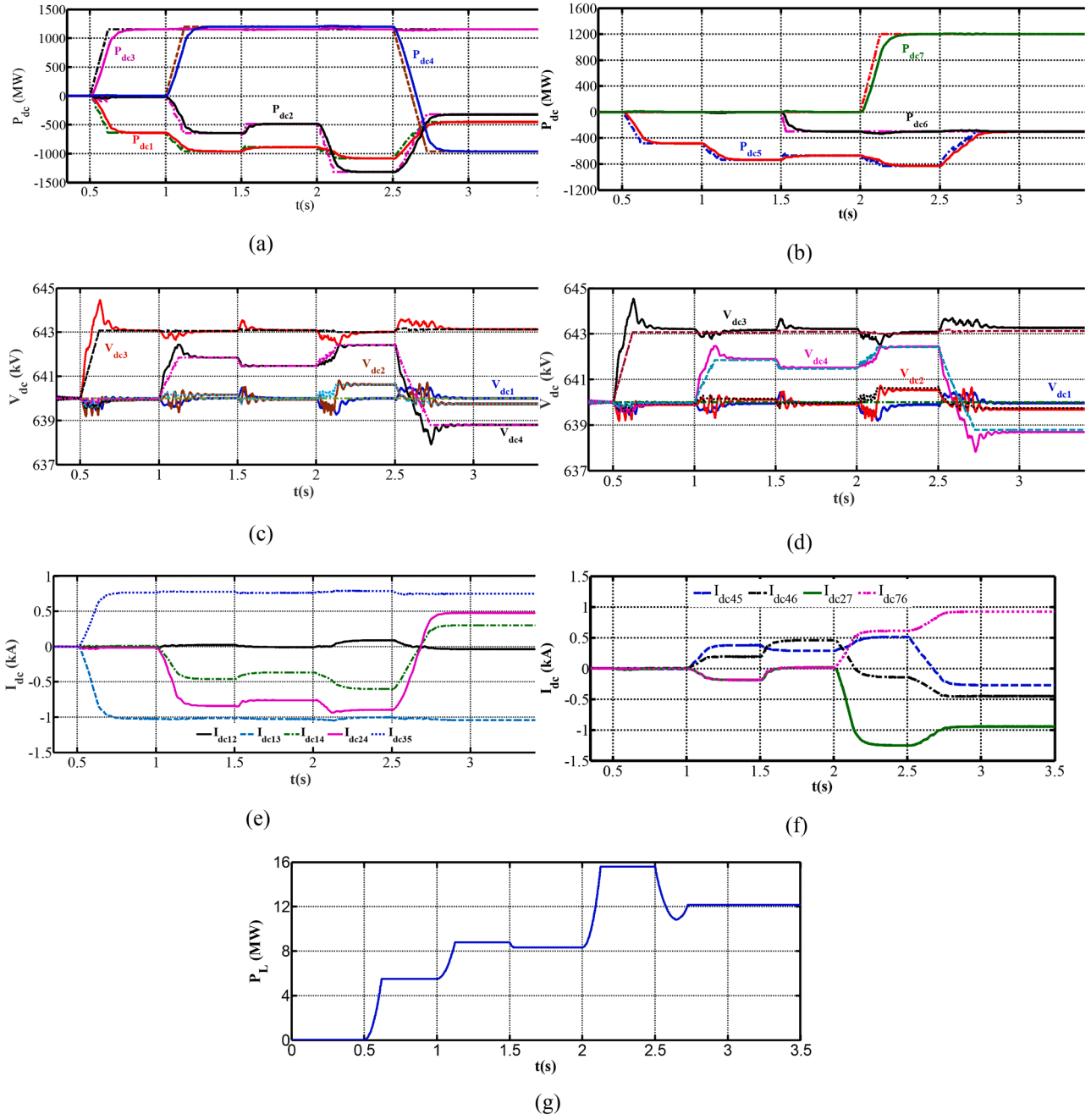

Fig. 5. Waveforms that illustrate the performance of the optimization based dc grid controller being studied during normal operation, where (a) and (b) are dc powers of the VSC_1 to VSC_7; (c) and (d) are dc voltages of the VSC_1 to VSC_7; (e) and (f) are dc currents of the dc cables that link the converter terminals; and (g) is the plot for the total power loss as the power set-points at converter terminals vary.

powers (or currents) are routed through the shortest electrical paths '2′ and '5′ to ensure minimum power loss, with no dc currents observed in the other dc cables.

The plots for the dc cable currents in Fig. 5(e) and (f) indicate that the optimizer minimizes the power losses by ensuring the current flows in the dc cables with higher resistances (longer lengths) such as dc cable '1′ are minimized. Similar behavior is observed in the subsequent periods, with Fig. 5(g) displaying total dc network power loss '$P_L(t)$' as the power exchange varies. Since dc power flow in a mesh network is highly sensitive to changes in dc cable resistances, the sensitivity of the presented dc grid controller to changes in dc cables' resistances is examined, assuming the followings: dc cable temperature change, $\Delta t = 15C^o$; Aluminum dc cable with temperature coefficient, $\alpha = 4.308$ per C^o; and initial resistance, $R_0 = 10\text{m}\Omega/\text{km}$, and operating conditions remain the same as stated above. The dc powers and dc voltages displayed in Fig. 6 (a) to (d) show that the actual (measured) dc voltages of converter terminals exhibit small drift from the optimal dc voltages in favor of tracking the optimal dc power set-points. This is because of the added droops in Fig. 2, which are practically proportional controller having succeeded in forcing the dc powers to follow their optimal set-points. These results demonstrate the resiliency of the presented optimization based dc grid control to potential parameter variation.

3.2. HVDC network reconfiguration

This part assesses the performance of the proposed optimization

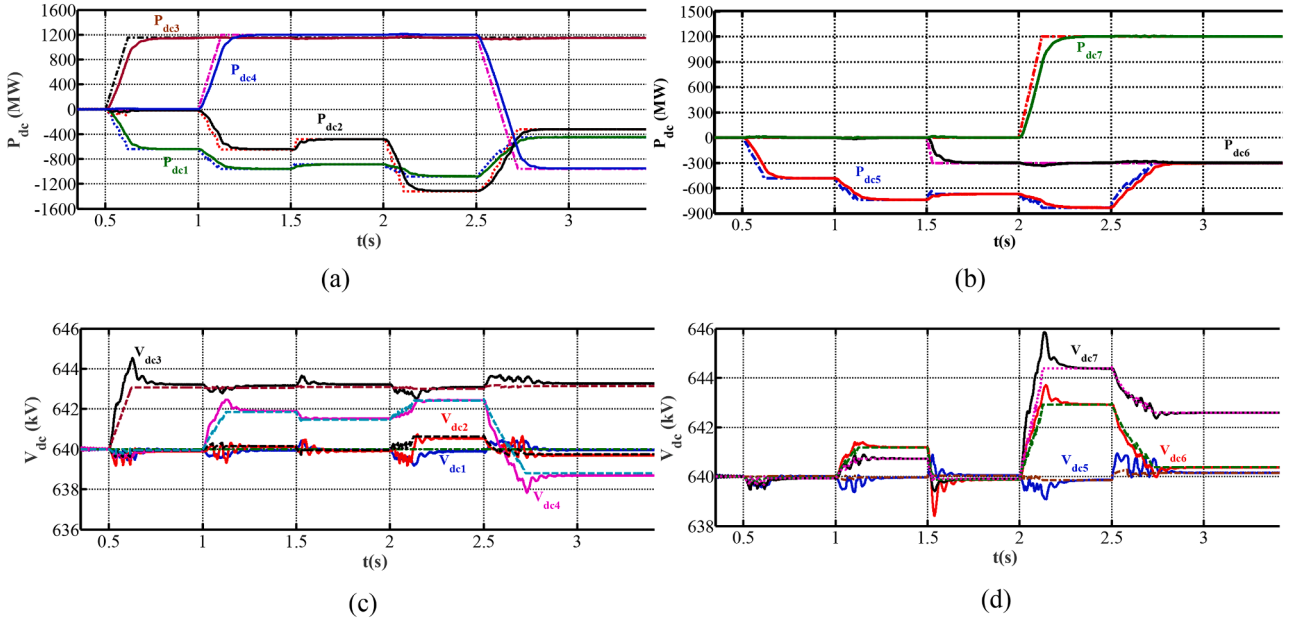

Fig. 6. Selected waveforms that illustrate the resilience of the presented optimization dc grid controller as dc cable resistance varies with temperature changes, where (a) and (b) are dc powers of the VSC_1 to VSC_7; and (c) and (d) are dc voltages of the VSC_1 to VSC_7.

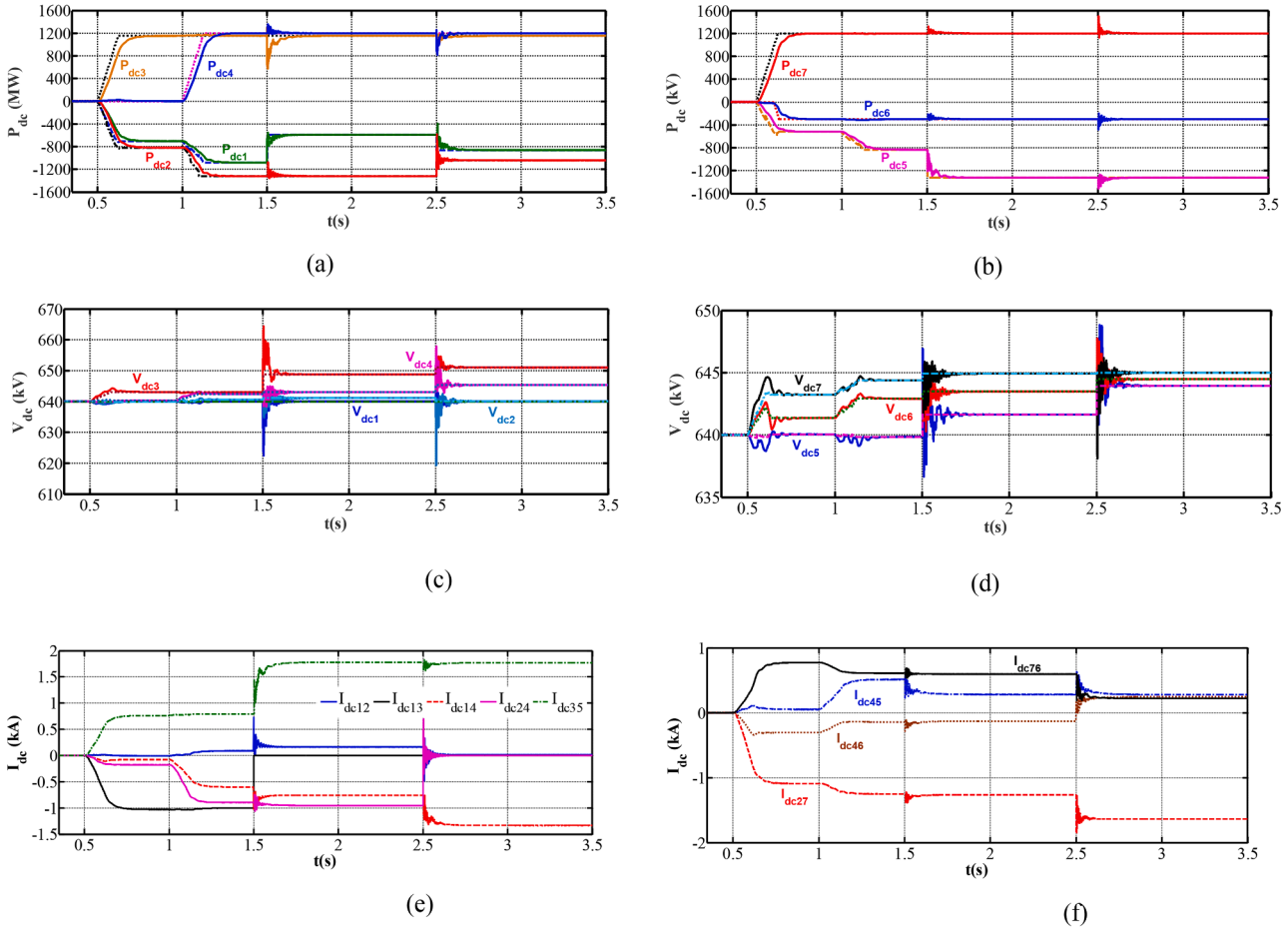

Fig. 7. Waveforms that illustrate autonomous rerouting of the dc power during dc cable outages, where (a) and (b) are dc powers of the VSC_1 to VSC_7; (c) and (d) are dc voltages of the VSC_1 to VSC_7; and (e) and (f) are dc currents of the dc cables that link the converter terminals.

based dc grid controller during dc cable outage, with particular emphasis on the optimal rerouting of the dc powers toward dispatch centres. The system operating conditions in this assessment are summarized as follows:

- Initially, all converters held their dc powers to zero, and at $t = 0.5$ s VSC3, VSC6 and VSC7 ramp their dc output powers gradually from 0 to 1152MW, −300MW and 1200MW, and the dc powers are maintained at these values for the rest of the simulation period.
- At $t = 1$ s, VSC4 gradually increases its dc power output to 1200MW which is maintained for the rest of the simulation period.
- Initially, all dc circuit breakers were closed, and at $t = 1.5$ s and $t = 2.5$ s, the permanent loss of dc lines '1′ and '2′ in Fig. 1 were simulated by opening the dc circuit breakers at their ends [42] .

Fig. 7(a) - (f) show that the proposed optimization based dc controller has successfully adjusted the optimal set-points (dc powers and dc voltages) and provided to converter terminal controllers in order to ensure stable operation of the multi-terminal HVDC network. Recall that the proposed dc grid controller has exploited the status signals of the dc circuit breakers of different dc lines to modify the conductance matrix as circuit topology of the dc network varies in order to estimate optimal set-points. The plots for dc powers and dc currents in Fig. 7(a) and (b), and Fig. 7(e) and (f) show that the converter terminals without prescribed dc powers (VSC_1, VSC_2 and VSC_5) have established new optimal dc powers as a result of outage of dc lines '1′ and '2′, with the current flow in the affected dc lines (I_{dc12} and I_{dc13}) dropping to zero as expected. These plots also show the proposed dc controller can autonomously work out the new optimal routes for power flow every time new dc line is subjected to the outage. Fig. 7(c) and (d), and Fig. 7(e) and (f) show that despite the loss of two critical lines, the converter dc link voltages and currents in all dc cables are within permissible limits for continuous operation.

3.3. HVDC network reconfiguration with running cost minimization

This part repeats the studies performed in subsection III-0, but this time the dc cables '2′ and '5′ are permanently lost at $t = 1.5$ s and 2.5 s, and with the objective function of minimizing the system running cost when rerouting the dc powers toward dispatch centres. The dc powers

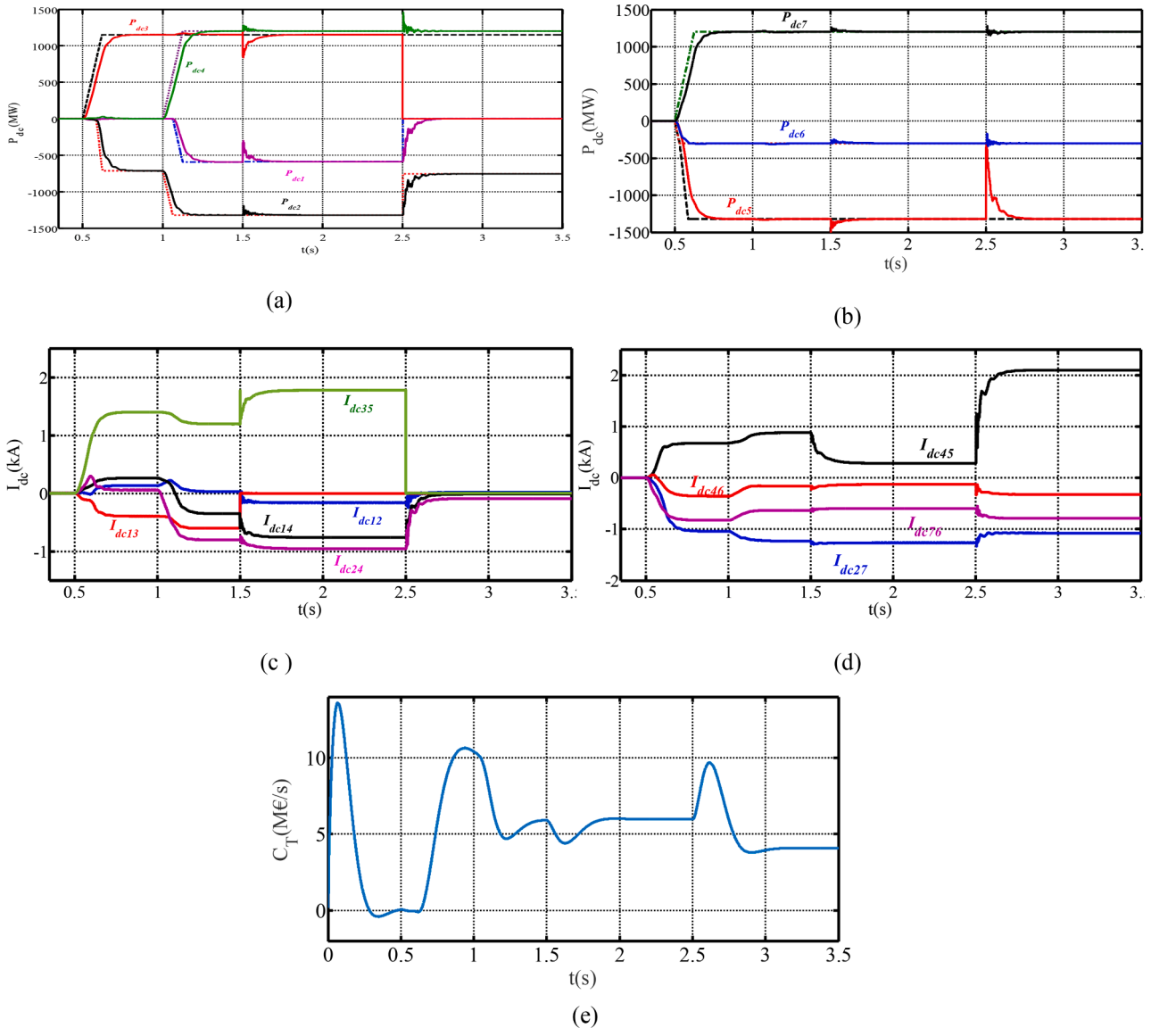

Fig. 8. Waveforms that illustrate autonomous rerouting of the power when system running cost is minimized, where (a) and (b) are dc powers of the VSC_1 to VSC_7; (c) and (d) are dc currents of the dc cables that link the converter terminals; and (e) is the plot for the running cost as the power set-points at converter terminals vary.

and currents plots in Fig. 8(a) and (b), and (c) and (d) show that the loss of the dc cable 2 at t= 1.5 s has not resulted in the change of the optimal set-points, with the dc current (or power transfer) in the longest dc cable between VSC_1 and VSC_2 remains minimal. After the loss of dc cable 5, which resembles a permanent loss of VSC_3, VSC_1 reduces its dc power to zero, while VSC_2 adjusts its dc power to maintain the power balance between ac and dc sides, see Fig. 8(a) and (b). The plots in Fig. 8(a) and (b) and (c) and (d) indicate that the optimizer operates VSC_2 and VSC_5 at their thermal limits in favor of not violating the specified dc cables overload limits. The plots in Fig. 8(a) and (b) and (c) show the fall of the dc currents I_{dc13} and I_{dc35} and of the dc power injection from VSC_3 to zero subsequent the loss of the lines '2′ and '5′ as anticipated. Observe that after the loss of VSC_3 and its dc power, the total dc grid power mismatch is being provided by VSC_2 and VSC_5 as the dc grid optimizer forces the dc power of the VSC_1 to zero in order to minimize the running cost. Forcing dc power of VSC_1(which 200 km from VSC_4) to zero instead of that of the VSC_5 (which is 250 km from VSC_4) is a clear evidence of the energy pricing in different ac networks have greater influences in the outcome of optimization. The optimal running cost that takes into account the transmission losses and price differences in different ac networks is displayed in Fig. 8(e). This plot shows that the global solution for optimal running varies with the operating points of the active power controlling converters.

4. Conclusion

To optimize operation and prevent overloading of key components such as dc lines and converter stations, this paper has presented a dc grid controller capable of optimizing the performance of highly meshed multi-terminal HVDC networks for a number of operational objectives such as transmission efficiency, running cost, etc. The presented dc grid controller performs online optimization in each sample time to estimate the optimal power or dc voltage set-points to be provided to converter terminals. Its theoretical formulation has been discussed and validated using MATLAB simulations. It has been shown that the incorporation of the dc power-dc voltage droops and knowledge of dc circuit breaker status can improve the tracking speeds of the optimal set-points during normal operation and dc network reconfiguration, with the former improve the immunity (reduce sensitivity) of the proposed dc grid controller to dc grid parameter variations. Therefore, it could be concluded that the presented dc grid controller is promising for the operation of complex dc grids with a large number of converter terminals. The outstanding work is experimental corroboration of the proposed dc grid controller on small-scale protype or replica of highly meshed dc grid.

Authors statement

We would like to declare that this manuscript is not is submitted for consideration to any other journal or conference. To the best of our knowledge, the entire contents of this manuscript are results of original research works conducted by the authors as part of collaboration between NEOM and King Abdulaziz University.

Many thanks

Dr G.P. Adam, PhD, MSC, BSc, MIEEE and Member of Power Electronics Society, NEOM.com, Lead Engineer, Associate Editor in IEEE Journal of Emerging and Selected Topics in Power Electronics (JESTPE)

Declaration of Competing Interest

The authors would like to declare they have conflict of interest, knowingly or unknowingly, with any member of editorial team of the Journal of Electric Power Systems Research nor any party that can be considered as conflict of interest or involved in promotion of unethical behaviours which are contrary to the values of the journal, and letter and spirit of scientific research.

Acknowledgement

The authors extend their appreciation to the Deputyship for Research & Innovation, Ministry of Education in Saudi Arabia for funding this research work through the project number (1034).

References

[1] W. Feng, Q. Shi, H. Cui, F. Li, Optimal power allocation strategy for black start in VSC-MTDC systems considering dynamic impacts, Electr. Power Syst. Res. 193 (2021), 107023. /04/01/2021,In this issue.
[2] H. Dadgostar, M. Hajian, K. Ahmed, DC grids DC fault detection using asymmetric pole inductors, Electr. Power Syst. Res. 193 (2021), 107016. /04/01/2021,In this issue.
[3] J. Kayser, S. Schlegel, D. Westermann, An advanced control strategy for DC interconnections of distribution systems considering curative system security, Electr. Power Syst. Res. 189 (2020), 106652. /12/01/2020, In this issue.
[4] S.D. Tavakoli, E. Sánchez-Sánchez, E. Prieto-Araujo, O. Gomis-Bellmunt, DC voltage droop control design for MMC-based multiterminal HVDC grids, IEEE Trans. Power Delivery 35 (5) (2020) 2414–2424. In this issue.
[5] S. Balasubramaniam, C.E. Ugalde-Loo, J. Liang, T. Joseph, A. Adamczyk, Pole balancing and thermal management in multiterminal HVdc grids using single H-Bridge-based current flow controllers, IEEE Trans. Indust. Electron. 67 (6) (2020) 4623–4634. In this issue.
[6] S. Wang, K.H. Ahmed, G.P. Adam, A.M. Massoud, B.W. Williams, A novel converter station structure for improving multiterminal HVDC system resiliency against AC and DC faults, IEEE Trans. Indust. Electron. 67 (6) (2020) 4270–4280. In this issue.
[7] Y. Wen, C.Y. Chung, Z. Shuai, L. Che, Y. Xiao, X. Liu, Toward flexible risk-limiting operation of multi-terminal HVDC grids with vast wind generation, IEEE Trans. Sustainable Energy 11 (3) (2020) 1750–1760. In this issue.
[8] J.C. Gonzalez-Torres, G. Damm, V. Costan, A. Benchaib, F. Lamnabhi-Lagarrigue, A novel distributed supplementary control of multi-terminal VSC-HVDC grids for rotor angle stability enhancement of AC/DC systems, IEEE Trans. Power Syst. 36 (1) (2021) 623–634. In this issue.
[9] R. Zeng, L. Xu, L. Yao, B.W. Williams, Design and operation of a hybrid modular multilevel converter, IEEE Trans. Power Electron. 30 (3) (2015) 1137–1146. In this issue.
[10] C. Barker, R. Whitehouse, J. Lang, S. Wang, Risk of multiple cross-over of control characteristics in multi-terminal HVDC, IET Generation, Transmission & Distribution 10 (6) (2016) 1353–1360. In this issue.
[11] U.N. Gnanarathna, A.M. Gole, R.P. Jayasinghe, Efficient modeling of modular multilevel HVDC converters (MMC) on electromagnetic transient simulation programs, IEEE Trans. Power Delivery 26 (1) (2011) 316–324. In this issue.
[12] Y. Ye, Y. Qiao, L. Xie, Z. Lu, A comprehensive power flow approach for multi-terminal VSC-HVDC system considering cross-regional primary frequency responses, J. Mod. Power Syst. Clean Energy 8 (2) (2020) 238–248. In this issue.
[13] M. Goertz, S. Wenig, S. Beckler, C. Hirsching, M. Suriyah, T. Leibfried, Overvoltage characteristics in symmetrical monopolar HB MMC-HVDC configuration comprising long cable systems, Electr. Power Syst. Res. 189 (2020), 106603. /12/01/2020,In this issue.
[14] Y. Zhang, W. Cong, G. Li, K. Sun, Y. Zhang, Single-ended MMC-MTDC line protection based on dual-frequency amplitude ratio of traveling wave, Electr. Power Syst. Res. 189 (2020), 106808. /12/01/2020,In this issue.
[15] L. Tang, B.-.T. Ooi, Locating and isolating DC faults in multi-terminal DC systems, IEEE Trans. on Power Delivery 22 (3) (2007) 1877–1884. In this issue.
[16] D. Vozikis, V. Psaras, F. Alsokhiry, G.P. Adam, Y. Al-Turki, Customized converter for cost-effective and DC-fault resilient HVDC Grids, Int. J. Electr. Power Energy Syst. 131 (2021), 107038. /10/01/2021,In this issue.
[17] A. Nami, J. Liang, F. Dijkhuizen, G.D. Demetriades, Modular Multilevel Converters for HVDC Applications: review on Converter Cells and Functionalities, IEEE Trans. Power Electron. 30 (1) (2015) 18–36. In this issue.
[18] G.P. Adam, K.H. Ahmed, B.W. Williams, Mixed cells modular multilevel converter. 2014 IEEE 23rd International Symposium On Industrial Electronics, pp. 1390–1395, ISIE, 2014 doi:10.1109/ISIE.2014.6864817.In this issue.
[19] J.A. Ansari, C. Liu, S.A. Khan, MMC based MTDC grids: a detailed review on issues and challenges for operation, control and protection schemes, IEEE Access 8 (2020) 168154–168165. In this issue.
[20] J. Renedo, A. Garcia-Cerrada, L. Rouco, L. Sigrist, Coordinated Design of Supplementary Controllers in VSC-HVDC Multi-Terminal Systems to Damp Electromechanical Oscillations, IEEE Trans. Power Syst. 36 (1) (2021) 712–721. In this issue.
[21] L. Shi, G.P. Adam, R. Li, L. Xu, Enhanced control of offshore wind farms connected to MTDC network using partially selective DC fault protection, IEEE J. Emerg. Sel. Top Power Electron. 9 (3) (2021) 2926–2935. In this issue.
[22] Z. Wang, J. He, Y. Xu, F. Zhang, Distributed control of VSC-MTDC systems considering tradeoff between voltage regulation and power sharing, IEEE Trans. Power Syst. 35 (3) (2020) 1812–1821. In this issue.
[23] J. Beerten, S. Cole, R. Belmans, Modeling of multi-terminal VSC HVDC systems with distributed DC voltage control, IEEE Trans. Power Syst. 29 (1) (2014) 34–42. In this issue.
[24] T. Nakajima, S. Irokawa, A control system for HVDC transmission by voltage sourced converters, 1999 IEEE Power Engineering Society Summer Meeting. Conference Proceedings (Cat. No.99CH36364) 2 (1999) 1113–1119, vol.2,In this issue.

[25] M. Han, D. Xu, L. Wan, Hierarchical optimal power flow control for loss minimization in hybrid multi-terminal HVDC transmission system, CSEE J. Power Energy Syst. 2 (1) (2016) 40–46. In this issue.
[26] J. Cao, W. Du, H.F. Wang, An improved corrective security constrained OPF for meshed AC/DC grids with multi-terminal VSC-HVDC, IEEE Trans. Power Syst. 31 (1) (2016) 485–495. In this issue.
[27] J. Cao, W. Du, H.F. Wang, S.Q. Bu, Minimization of transmission loss in meshed AC/DC grids with VSC-MTDC networks, IEEE Trans. Power Syst. 28 (3) (2013) 3047–3055. In this issue.
[28] S. Chondrogiannis, M.P. Blanco, Market integration scheme of a multi-terminal HVDC grid in the North Seas, IEEE Trans. Power Syst. 31 (3) (2016) 2415–2422. In this issue.
[29] M. Baradar, M.R. Hesamzadeh, M. Ghandhari, Second-order cone programming for optimal power flow in VSC-type AC-DC grids, IEEE Trans. Power Syst. 28 (4) (2013) 4282–4291. In this issue.
[30] L. Xu, L. Yao, DC voltage control and power dispatch of a multi-terminal HVDC system for integrating large offshore wind farms, Renew. Power Generation, IET 5 (3) (2011) 223–233. In this issue.
[31] G. Li, Z. Du, C. Shen, Z. Yuan, G. Wu, Coordinated design of droop control in MTDC grid based on model predictive control, IEEE Trans. Power Syst. PP (99) (2017) 1. In this issue.
[32] K. Rouzbehi, A. Miranian, J.I. Candela, A. Luna, P. Rodriguez, A generalized voltage droop strategy for control of multiterminal DC grids, IEEE Trans. Ind. Appl. 51 (1) (2015) 607–618. In this issue.
[33] P. Wang, S. Feng, P. Liu, N. Jiang, X.P. Zhang, Nyquist stability analysis and capacitance selection for DC current flow controllers in meshed multi-terminal HVDC grids, CSEE J. Power Energy Syst. 7 (1) (2021) 114–127.
[34] G.P. Adam, T.K. Vrana, R. Li, P. Li, G. Burt, S. Finney, Review of technologies for DC grids – power conversion, flow control and protection, IET Power Electron. 12 (8) (2021) 1851–1867. Available:In this issue.
[35] C. Gong, S. Yao, Y. Wang, H. Guo, The study and application of power flow controller for DC grids. International Conference on Renewable Power Generation, EC Accession Number: 15796081 DOI: 10.1049/cp.2015.0560, pp. 1–5, RPG, 2015, 2015,In this issue.
[36] S. Balasubramaniam, J. Liang, C.E. Ugalde-Loo, An IGBT based series power flow controller for multi-terminal HVDC transmission. 2014 49th International Universities Power Engineering Conference,10.1109/UPEC.2014.6934626, pp.1–6, UPEC, 2014.
[37] T. Zhang, C. Li, J. Liang, A thyristor based series power flow control device for multi-terminal HVDC transmission. 2014 49th International Universities Power Engineering Conference,10.1109/UPEC.2014.6934802, pp.1–5, UPEC, 2014.
[38] J. Sau-Bassols, E. Prieto-Araujo, O. Gomis-Bellmunt, F. Hassan, Selective Operation of Distributed Current Flow Controller Devices for Meshed HVDC Grids, IEEE Trans. Power Delivery 34 (1) (2019) 107–118, https://doi.org/10.1109/TPWRD.2018.2848547. In this issue.
[39] J. Sau-Bassols, E. Prieto-Araujo, O. Gomis-Bellmunt, Modelling and Control of an Interline Current Flow Controller for Meshed HVDC Grids," in, IEEE Transactions on Power Delivery 32 (1) (Feb. 2017) 11–22, https://doi.org/10.1109/TPWRD.2015.2513160.
[40] N. Ahmed, et al., Efficient modeling of an MMC-based multiterminal DC system employing hybrid HVDC breakers, IEEE Trans. Power Del. 30 (4) (2015) 1792–1801. In this issue.
[41] F.B. Ajaei, R. Iravani, Enhanced equivalent model of the modular multilevel converter, IEEE Trans. Power Delivery 30 (2) (2015) 666–673. In this issue.
[42] R. Li, L. Xu, L. Yao, DC fault detection and location in meshed multiterminal HVDC systems based on DC reactor voltage change rate, IEEE Trans. Power Delivery 32 (3) (2017) 1516–1526. In this issue.